Proceedings of the 21st ICSMGE, Vienna, Austria, 14 – 19 June 2026. Pistrol, Adam & Schweiger (eds.)
Published by: ÖGG, Austrian Society for Geomechanics, Salzburg, Austria, ISBN 978-3-9503898-4-5
https://doi.org/10.53243/ICSMGE2026-1980

Effect of pile geometry during installation of model offshore monopiles

David León-Vanegas, Marcos Arroyo
Universitat Politècnica de Catalunya – BarcelonaTech UPC, Barcelona, Spain, david.eduardo.leon@upc.edu

Lluís Monforte
Centre International de Mètodes Numèrics en Enginyeria – CIMNE, Barcelona, Spain

ABSTRACT: Monopiles are typically installed using impact or vibration driving. In the installation process, the surrounding soil undergoes changes in stresses, density and in particle size distribution due to grain crushing. Despite the importance of soil state modification in the penetration response during installation, this remains an aspect with high uncertainty in driveability methodologies. In this work, the effect of pile geometries in the penetration resistance is investigated, using a numerical model based on the Geotechnical Particle Finite Element Method (G-PFEM) and a critical state constitutive model which incorporates the effect of the soil state in strength and compressibility. The model is first validated by simulating a cone penetration in a centrifuge test in a very fine silica sand. The findings demonstrate the ability of the numerical framework to adequately simulate the modification of soil state during monopile installation and highlight the changes produced in the soil state during the installation.

KEYWORDS: Monopile installation, driveability, G-PFEM, state parameter.

1 INTRODUCTION

Monopiles are the main foundation structure used for offshore wind turbines (OWT), and are usually installed using impact or vibration driving. In this process, the surrounding soil undergoes changes in stress, density and particle size distribution due to grain crushing and migration of fine crushing products. However, the effect of these changes on the penetration response during installation remains an aspect with high uncertainty in driveability methodologies, due to the difficulties of studying this problem using physical modelling or numerical modelling.

The numerical simulation of the pile driving presents numerous challenges because it comprises several non-linearities: geometric no-linearity due to large deformations, material no-linearity associated with the constitutive behavior of the surrounding soil and contact no-linearity arising from the interaction between the pile and the soil. Due to the large deformation involved in the numerical simulation of monopile driving, the conventional Lagrangian Finite Element Method (FEM) is not suitable for this task, as mesh distortion can occur, leading to inaccurate solutions or premature termination of the computation. Therefore, special numerical methods are required to model the pile installation process. Some of the methods used include the Coupled Eulerian Lagrangian method (Staubach et al., 2021), the Arbitrary Lagrangian Eulerian method (Spyridis et al., 2023), and the Material Point Method (MPM) (Galavi et al., 2024), among others.

An alternative to simulate the large deformation problem of monopile installation is the Geotechnical Particle Finite Element (G-PFEM), which has proved to be a successful tool for modelling large deformation insertion problems in geomechanics, such as simulation of CPTu (Monforte et al., 2021) and soil sampling (Monforte et al., 2022).

In this work the G-PFEM is used alongside a critical state based constitutive model that consider the effect of soil density in the strength and compressibility, to simulate the installation of monopiles by monotonic jacking in a dry very fine UWA (University of Western Australia) silica sand. The paper is structured in two main sections: The first one presents the general description of the G-PFEM, followed by the constitutive relations used for the simulations. In the second one, the description of the centrifuge test performed by Fan et al (2021) used for validation is presented, following by the numerical results using the G-PFEM. The effect of the model monopile geometry is then examined in detail.

2 NUMERICAL MODEL

This section addresses the numerical algorithms employed. First, a brief review of the G-PFEM is presented. Second, the formulation in a large strain framework of the SIMSAND model used for the simulations is presented. For details regarding the algorithms and formulation method of the G-PFEM, the reader is referred to (Carbonell et al., 2022).

2.1 *Geotechnical Particle Finite Element Method G-PFEM*

The Particle Finite Element Method PFEM is a method that uses an updated Lagrangian description of motion and treats the finite element nodes as particles. These particles are used to construct a finite element mesh in each time-step, guaranteeing a good mesh quality and an optimal solution. The Geotechnical Particle Finite Element Method G-PFEM implementation (Carbonell et al., 2022) uses low-order linear stabilized finite elements (Monforte et al., 2017) and includes stabilized coupled hydromechanical formulation for quasi-static and dynamic conditions (Monforte et al., 2017).

2.2 *Constitutive model*

A modified version of the critical state based SIMSAND model developed by Jin et al (2017) has been used to describe the stress and state dependent behaviour of sand. This constitutive model has been implemented in G-PFEM using a large-strain elasto-plastic framework, wherein the deformation gradient is divided multiplicatively into an elastic and a plastic part. For the sake of simplicity, the constitutive model is briefly described here in terms of stress invariants.

The elastic deformation is assumed to follow the hyperelastic model defined by Houlsby et al. (2005), in which the Gibss complementary energy is defined according to Equation (1).

$$E = \frac{p_0^{2-n}}{p_a^{1-n} k(1-n)(2-n)} - \frac{p}{k(1-n)}$$
$$p_0^2 = p^2 + \frac{k(1-n)q^2}{3g} \quad (1)$$

where, P_a is a reference pressure, k is the bulk stiffness factor, g is the shear stiffness factor, n is a pressure exponent and p_0 is a function of stresses that consider both the mean effective

stress p and the deviatoric stress invariant q of the Kirchhoff stress tensor.

The yield surface in the $p-q$ space is a wedge defined by the following equation.

$$f = \frac{q}{p} - \frac{M_p\,\epsilon_d^p}{k_p + \epsilon_d^p} \tag{2}$$

where, M_p is the available peak stress ratio, ϵ_d^p is the Hencky deviatoric plastic strain and k_p is a material parameter that controls the plastic stiffness.

The model uses a nonlinear stress-dilatancy relationship generalizing a Roscoe-type dilatancy rule.

$$\frac{\delta\epsilon_v^p}{\delta\epsilon_d^p} = A_d\left(M_{ph} - \frac{q}{p}\right) \tag{3}$$

where, A_d is a parameter that controls the magnitude of stress-dilatancy and M_{ph} is the phase transformation ratio. M_p and M_{ph} are defined to be function of the critical state ratio M_θ and the state parameter ψ of Been and Jefferies (1985) using the following exponential expressions, where n_p and n_d are materials parameters.

$$\begin{aligned} M_p &= M_\theta\, exp(-n_p\psi) \\ M_{ph} &= M_\theta\, exp(n_d\psi) \end{aligned} \tag{4}$$

The stress ratio at critical state M_θ varies with Lode's angle according to the smooth function in the deviatoric plane defined by Sheng et al. (2000).

As presented in Equation (5), the Critical State Line in the model is non-linear in the semi-logarithm compression plane and follows the exponential form defined by Gudehus (1997).

$$e_{cs} = e_{c0}\, exp\left(-\lambda'\left(\frac{p'}{p_a}\right)^{\xi}\right) \tag{5}$$

where, e_{c0} is the critical void ratio for zero mean effective stress, λ' controls the position of the inflection point and ξ controls the slope after the inflection point.

3 RESULTS

Initially the model was calibrated for the UWA silica sand based on experimental test. Then, the accuracy of the numerical model was validated against measured cone resistances from the centrifuge tests by Fan et al. (2021). Finally, the effect of model monopile geometry was evaluated.

3.1 *Calibration of the constitutive model*

The UWA silica sand is a very fine sand with a mean size d_{50} of approximately 0.17 mm and a sub-rounded to sub-angular grain shape.

The calibration of the SIMSAND model for this sand was done based on the different experimental test published in the characterization report by Chow et al. (2019). A preliminary set of parameters were set with the interpretation of the drained triaxial test and then an adjustment of those were carried out by simulating the elementary test in G-PFEM. Table 1 summarizes the parameters, while Figure 1 shows the comparation of the experimental results with the numerical outputs.

Table 1. Parameters of the SIMSAND model for UWA silica sand.

Parameter	Value	Unit
Reference pressure: p_a	100.0	kPa
Bulk stiffness factor: k	267	-
Shear stiffness factor: g	200	-
Pressure exponent: n	0.70	-
Plastic modulus: k_p	0.0025	-
Stress-dilatancy parameter: A_d	0.55	-
Exponent of mobilized peak ratio: n_p	1.6	-
Exponent of dilatancy ratio: n_d	3.0	-
Critical stress ratio: M	1.29	-
Critical void ratio at p=0: e_{c0}	0.755	-
CSL position: λ	0.008	-
CSL slope: ξ	0.98	-

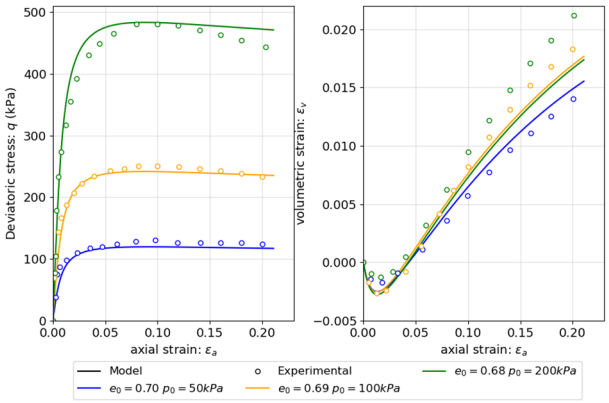

Figure 1. Drained triaxial test in UWA silica sand. Experimental results and numerical simulations.

3.2 *Cone penetration simulation*

The validation of the numerical model was made based on the simulation of the 7 mm diameter cone penetration test performed in the centrifuge tests by Fan et al. (2021) at 100 g.

Due to the symmetry of the problem, an axisymmetric model was used. Figure 2 shows the G-PFEM model considering the prototype dimensions. Linear triangle elements with a stabilized mixed formulation - that include the Jacobian as additional degree of freedom - were used to improve the accuracy of the solution (Monforte et al., 2017).

The cone was considered a rigid body. The interaction between the cone and the soil domain was defined using a penalty contact with Coulomb friction. A contact friction angle of 6º was assumed, corresponding to a fraction of 0.20 of the sand critical friction angle. This choice is consistent with the relatively smooth surface and aligns with recent simulations of CPT in sand (Boschi et al., 2024).

A sensitivity analysis of the initial void ratio of the sand was also performed. The cone tip resistance q_c measured in the centrifuge test and the one obtained in the numerical simulations for the different e_0 is presented in Figure 3. These numerical outputs show a good agreement of q_c for depths greather than 5.0 m and $e_0 = 0.72$, suggesting that this was the initial void ratio of the sand sample in the centrifuge box. This initial void ratio corresponds to a loose to medium dense sand, according to the minimum and maximum void ratios measured in laboratory (Chow et al., 2019).

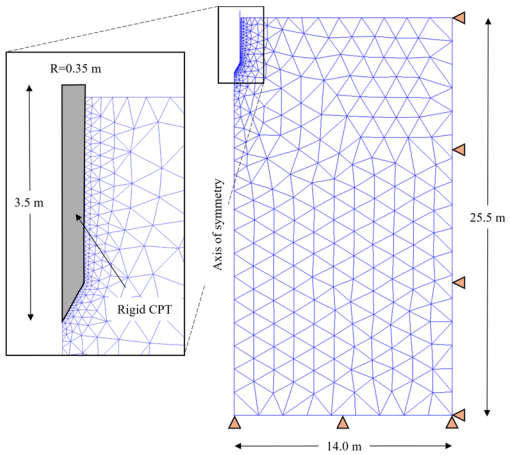

Figure 2. Axisymmetric model for D=0.7 m CPT.

It is important to clarify that, in order to facilitate contact definition at the outset of the simulation, the numerical simulation of the CPT started with an initial embedded of 3.5 m. Therefore, the numerical results for the first 5.0 m are not considered representatives.

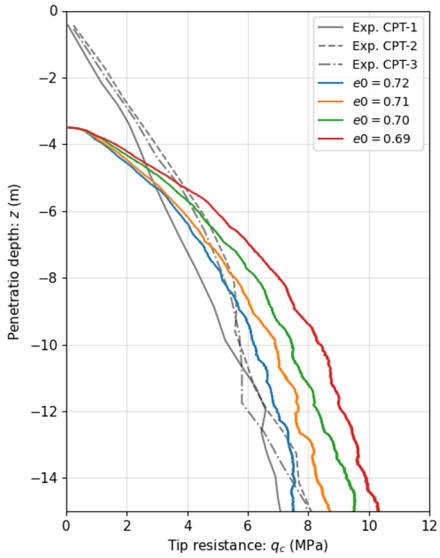

Figure 3. Cone tip resistance profile from experimental tests and numerical model.

3.3 *Monopile installation simulation*

To study the effect of pile geometry in monopile installation, a simulation was conducted using the G-PFEM for a 5 m diameter open-ended pile with a wall thickness of 0.1 m installed by monotonic jacking. This problem was also studied in the centrifuge test by Fan et al. (2021) at 100 g.

Similar to the cone model, an axisymmetric model with stabilized linear triangle elements were used. Three geometries conditions were considered: First, the detailed geometry used by Fan et al. (2021) presented in Figure 4 that includes the epoxy installed to protect the strain gauges, leading to an overall diameter (D) and wall thickness (t) of 5.22 m and 0.21 m, respectively. Second, a constant wall thickness t = 0.1m and D = 5.0 m. Third a constant t = 0.21 m and D = 5.22 m.

A contact friction angle δ = 6 º was assumed for the pile internal wall considering that the material is extruded stainless steel. Whereas, according to Fane t al., (2021) a δ =15º was used for the epoxy used in the pile external wall surface.

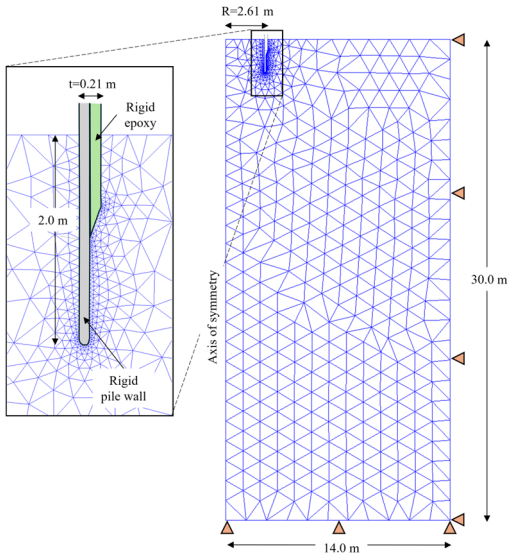

Figure 4. Axisymmetric model for D=5.22 m monopile.

Figure 5 depicted the normalized penetration resistance (penetration resistance over the pile area) obtained for the numerical simulations. Analogous to the results of the cone test, the monopile was initial embedded 2.0 m, and the results for the first 3.0 m are not representative.

As presented in Figure 5, the numerical results for the detailed geometry follow the trend in the installation force measured in the centrifuge test. The minor discrepancies remaining between the numerical simulation and the centrifuge test are attributed to uncertainties in the contact friction angle in the inner and outer pile walls and the geometry of the epoxy installed on the external wall.

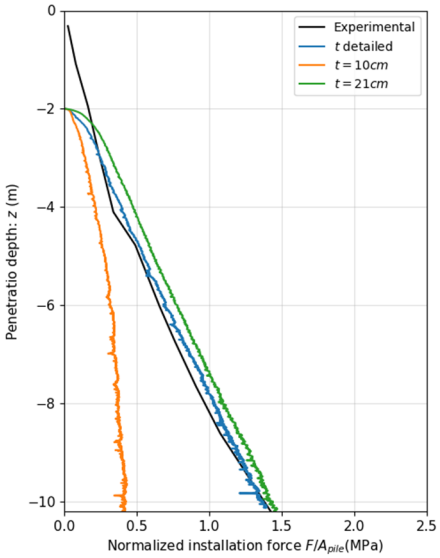

Figure 5. Normalized installation force during jacking installation of 5 m diameter monopile. Experimental and numerical outputs

The differences in penetration resistance for the three geometries are explained by the differences in the stresses and change in density produced during the installation. As presented in Figure 6, smaller radial stresses are generated and more local changes around the pile of void ratio are produced for the monopile with t = 0.1 m. In the other hand, higher stresses are produced and more important changes in the density around the pile shaft and in distance far from this are produced for the detailed geometry and the monopile with t = 0.21 m.

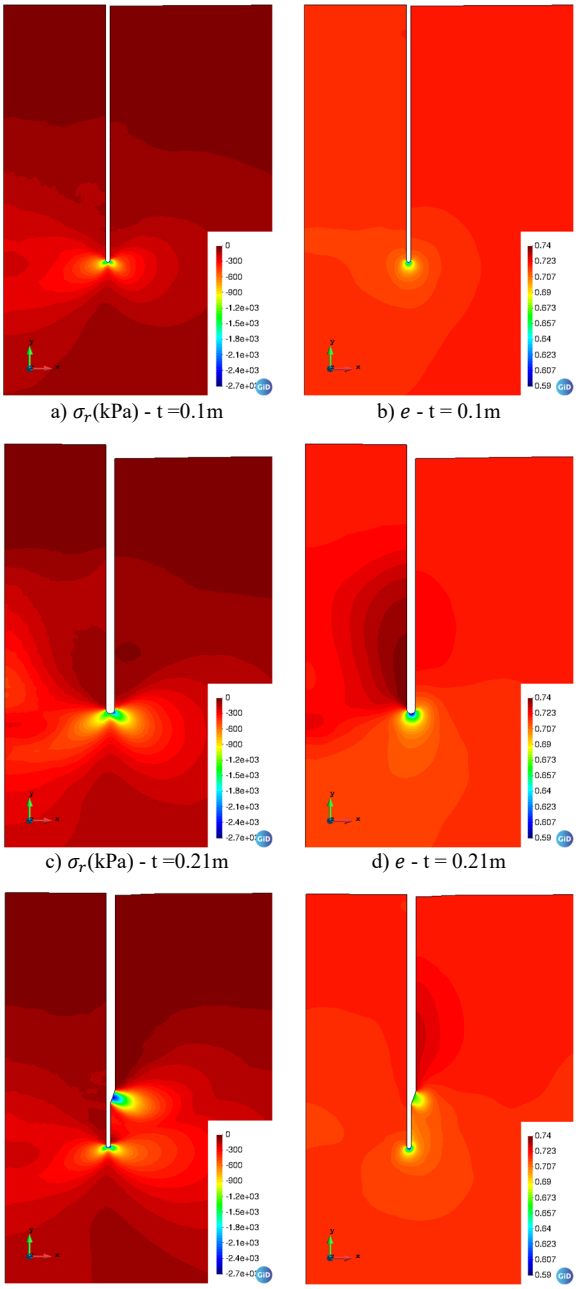

a) σ_r(kPa) - t =0.1m b) e - t = 0.1m

c) σ_r(kPa) - t =0.21m d) e - t = 0.21m

e) σ_r(kPa) - detailed geometry f) e - detailed geometry

Figure 6. Radial stress σ_r and void ratio e at 6.0 m of installation.

Particularly intriguing are the comparative outcomes of the detailed geometry and the one with constant t = 0.21 m. Although the former has a smaller pile tip, the radial stresses produced during installation are higher and affect a bigger area further away from the pile axis. This is explained by the epoxy installed in the external pile wall, which produces a cone apex shape, where soil recompression occurs on a soil already densified by the initial encounter with the pile tip.

It is worth mentioning that the installation method affects the stresses and density after installation, especially for driven installation, where there is cycling shearing in the interface and the inertia of the soil volume inside the pile affects the conditions of plugging. It is thus anticipated that important differences will be observed when driven installation is considered. This will be assessed in future works, taking into consideration the constitutive model developed by León-Vanegas et al. (2025), which accounts for the effect of grain crushing on the mechanical behaviour.

4 CONCLUSIONS

A numerical investigation of the effect of pile geometry in penetration resistance has been presented using G-PFEM and the SIMSAND model. It has been found that the numerical framework can accurately simulate the observed monopile installation response in a centrifuge, unveiling the corresponding soil state modifications. The numerical outputs show the influence of pile geometry on the change in stresses and void ratio during installation.

5 ACKNOWLEDGEMENTS

The first author is grateful for the financial support provided by the European Union 's Horizon Europe Programme under the Marie Skłodowska–Curie actions HORIZON-MSCA-2021-DN-01 call (Grant agreement ID: 101072360).

6 REFERENCES

Been, K. and Jefferies, M. 1985. A state parameter for sands. *Géotechnique*, *35*(2), 99–112.

Boschi, K., Arroyo, M., Monforte, L., Carbonell, J.M. and Gens, A. 2024. Coupled hydromechanical modelling of cone penetration in layered liquefiable soils. *Geotechnique* 75(3). 308-322.

Carbonell, J.M., Monforte, L., Ciantia, M. O., Arroyo, M. and Gens, A. (2022). Geotechnical particle finite element method for modeling of soil-structure interaction under large deformation conditions. *Journal of Rock Mechanics and Geotechnical Engineering*, *14*(3), 967–983.

Chow, S., Roy, A., Herduin, M., Heins, E., King, L., Bienen, B., O'Loughlin, C., Gaudin, C. and Cassidy, M. 2019. Characterization of UWA silica sand. University of Western Australia.

Fan S., Bienen B. and Randolph M.R. 2021. Centrifuge study on effect of installation method on lateral response of monopiles in sand. *Int. Journal of Physical Modelling in Geotechnics*, 21(1). 40-52.

Galavi, V and Martinelli M. 2024. MPM Simulation of the Installation of an Impact-Driven Pile in Dry Sand and Subsequent Axial Bearing Capacity. *Journal of Geotechnical and Geoenvironmental Engineering* 150(4).

Gudehus, G. 1997. Attractors, percolation thresholds and phase limits of granular soils, *Powders and Grains '97*. Behringer,R. P. and Jenkins, J. T (eds), Rotterdam, Balkema, pp 169–183

Houlsby G.T., Amorosi, A and Rojas, E. 2005. Elastic moduli of soils dependent on pressure: a hyperelastic formulation. *Geotechnique* 55(5).

Jin, Y.F, Wu, Z.X., Yin, Z.Y. and Shen J.S. 2017. Estimation of critical state-related formula in advanced constitutive modeling of granular material. *Acta geotechnica* 12(6). 1329-1351.

Leon-Vanegas, D., Monforte, L., Arroyo, M. and Gens, A. 2025. A constitutive model accounting for grain crushing in silica sand. *Proc. of 5th International Symposium on Frontiers in Offshore Geotechnics*. Nantes.

Monforte, L., Marcos, A., Carbonell, J.M. and Gens, A. 2022. Large-strain analysis of undrained smooth tube sampling. *Geotechnique* 72 (1), 61-77.

Monforte, L., Gens, A., Arroyo, M., Mánica, M. and Carbonell, J. M. (2021). Analysis of cone penetration in brittle liquefiable soils. *Computers and Geotechnics*, *134*.

Monforte, L., Carbonell, J. M., Arroyo, M., & Gens, A. (2017). Performance of mixed formulations for the particle finite element method in soil mechanics problems. *Computational Particle Mechanics*, *4*(3), 269–284.

Sheng D., Sloan, S.W. and Yu H.S. 2000. Aspect of finite element implementation of critical state models. *Computational mechanics* 26, 185-196

Spyridis M. and Lopez-Querol S. 2023. Numerical investigation of displacement pile installation in silica sand. *Computer and Geotechnics* 161.

Staubach P., Machacek J and Wichtmann T. 2021. Large-deformation analysis of pile installation with subsequent lateral loading: Sanisand vs. Hypoplasticity. *Soil Dynamics and Earthquake Engineering*, 151.